

Assessment of Multipath in Aeronautical Environments

Michael Lentmaier, Bernhard Krach, Thomas Jost, Andreas Lehner, and Alexander Steingass
German Aerospace Center (DLR), Institute of Communications and Navigation, Oberpfaffenhofen

ABSTRACT

In the last years the usage of Global Navigation Satellite Systems (GNSS) systems for aviation was a quickly growing field. In this context the problem of multipath reception becomes crucial as aviation demands high accuracy navigation based upon GNSS throughout all phases of flight and in particular with strong requirements for the approach and landing phase. To address this issue, simulations have been carried out on the basis of the satellite-to-aircraft navigation channel model developed by DLR in 2003, which was approved in February 2007 as major revision to recommendation ITU 682-1. A theoretical analysis based on the ground echo statistics is also performed, resulting in an approximation of the pseudo-range error distributions. This analysis gives an insight into the nature of the multipath threat of the aeronautical channel and confirms the observations made from the simulated error distributions.

1. INTRODUCTION

As aviation desires reliable, continuous, accurate and site-independent available navigation of aircrafts the future European Global Navigation Satellite Systems (GNSS) Galileo has risen the hope to be able to phase out old-fashioned aeronautical navigation systems like VHF Omni-directional Range (VOR), e.g., and to replace them by space based navigation services, as GNSS has the advantage to be available nearly throughout the whole world at nearly every time, whereas the availability of today's radio-navigation systems is limited (depending on the system) for certain regions. It is expected that a combination of the Global Positioning System (GPS), the future European Galileo system, Inertial Reference Systems (IRS) and augmented services is able to fulfil the regulatory requirement concerning the terms

- Accuracy
- Availability
- Continuity
- Integrity

in a way that the integrated system can serve as a sole means of navigation for aircraft in nearly all phases of flight, including even the highly demanding landing-phase, which today still has to be aided by systems like Instrument Landing Systems (ILS) or Microwave Landing Systems (MLS) for high categories (CAT I-III).

In the design phase of such a new system an assessment of its performance and errors has to be carried out, including an investigation of situations where the system performance may be degraded by outside influences. For a GNSS receiver reception of multipath is such a crucial situation, which is known to deteriorate the performance of the receiver.

ANASTASIA (Airborne New and Advanced Satellite Techniques & Technologies in A System Integrated Approach) is a European Commission Framework Programme (FP6) aiming to carry out research, evaluation and cost benefit analysis to define new navigation and communication technologies and avionics architectures suitable for aircraft operation in the future satellite based European Air Traffic Management environment for the corresponding future Communication, Navigation and Surveillance (CNS) functionality. Outputs are validated by theoretical analysis, mock-up evaluations and selected flight-testing. In order to assess the effect of multipath on aeronautical space based navigation, simulations have been carried out [1]. For this purpose a GNSS purely software-based end-to-end simulator has been programmed to use a high resolution aeronautical multipath channel model [2], which had been derived from a measurement campaign for the emulation of the channel impulse response in an aeronautical environment [3][4]. The simulator itself is able to simulate the behaviour of a complete GNSS receiver channel. This allows to determine pseudo-range errors as a measure of the influence of multipath.

Basically two scenarios are covered by the simulations, one air transport scenario, where an "A340" aircraft model is used, and one bizjet (business jet) scenario, where the model of a smaller bizjet-like aircraft type "VFW614" is used. Both basic scenarios are simulated by using the GPS L1 C/A signal structure as well as a future Galileo E5 BOC modulated signal, which is expected to be used by aviation and other SoL (Safety of Life) applications. The underlying receiver principle, that all simulations are based on, is the architecture of a standard GNSS receiver, which comprises a Costas Phase-Lock-Loop (PLL) and a non-coherent Delay-Lock-Loop (DLL). This gives comparable simulation results as this receiver architecture and configuration is used as reference in many publications.

As the landing phase is expected to be the most crucial flight phase concerning multipath, all simulations cover this expected worst-case scenario. An aircraft descent rate of 3.5 m/s is representative to the one of a standard ILS approach and is used for all simulated approaches. In order to identify critical satellite constellations, simulation results are presented as a function of satellite azimuth and elevation with respect to the heading of the plane. For the most critical values of these angles, more intensive simulations have been carried out. Based on these the maximum pseudo-range error and the error distribution during a given number of flights are investigated.

A theoretical analysis is then carried out, resulting in an approximation of the pseudo-range error distribution. This analysis gives an insight into nature of the multipath threat of the aeronautical channel and confirms the observations made from the simulation results.

2. AERONAUTICAL MULTIPATH CHANNEL MODEL

As a result of a measurement campaign in 2002 a high resolution multipath channel model for satellite-based aeronautical navigation was published in [3]. For the assessment of the multipath within the scope of this work this channel model has been implemented in the simulator. The referred model is developed especially for aircraft landing scenarios and is basically a time-variant tap-delay line model, which is driven by deterministic as well as stochastic processes. A general time-variant channel impulse response is given by

$$h(t) = \sum_{k=1}^N a_k(t) \cdot \delta(t - \tau_k(t)), \quad (1)$$

where N denotes the number of paths, $a_k(t)$ the weight process for path k and $\tau_k(t)$ its time variant delay δ denotes the Dirac function. The Aeronautical Satellite Channel Model (ASCM) comprises four taps (cp. Figure 1), a LOS tap without attenuation and delay, a zero delay path of a diffractive component, attenuated with respect to the first path, a constant delayed path of a fuselage reflection and a path originating from ground reflections, whose delay is altitude dependent.

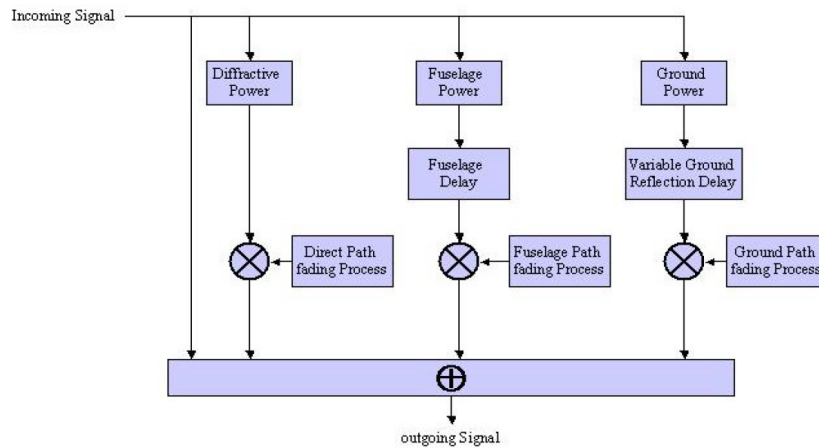


Figure 1: ASCM tap delay line impulse response

The characteristic of the ground echo depends thereby strongly on the current altitude. The ASCM distinguishes three different altitude zones that comprise four power levels respectively. The switching of the power levels is governed by a Markov model, whose transition probabilities depend on the airport environment. The ASCM is able to simulate an aircraft approach towards an airport with a constant sink rate. Depending on the current altitude level the ASCM uses a different transition matrix for switching between the power levels (see Figure 2). A MATLAB implementation of the ASCM is available for download [2]. A comparison of the ASCM with the International Civil Aviation Organization’s (ICAO) Standards and Recommended Practices (SARPs) error curve is given in [5].

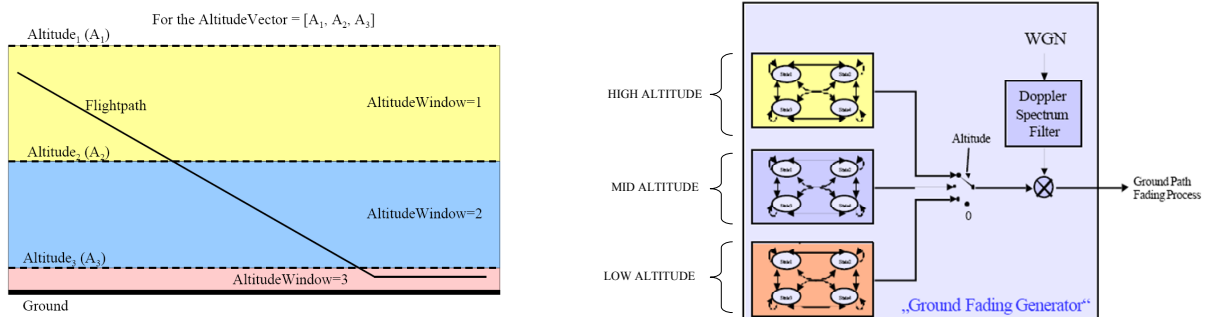


Figure 2: Illustration of aircraft flight path within the ASCM and associated ground fading generator

3. SIMULATION SCENARIOS

Basically two scenarios are covered by the simulations, an air transport scenario, where an “A340” aircraft model is used, and a bizjet scenario, where the model of a smaller bizjet-like aircraft type “VFW614” is used. Both basic scenarios are simulated by using the GPS L1 C/A signal structure as well as the future Galileo E5 AltBOC modulated signal.



(a) “VFW 614”



(b) “A340”

Figure 3: Aircraft types included within the ASCM

The ground fading parameters are set to the default values [2] for all simulations. The additional fourth altitude level (0-10m) is used shortly before the aircraft touches the ground. Please notice, that all simulations end here at the moment of the touchdown. It is further noted, that according to the measurement campaign in 2002 [3] done in order to create the model, no significant ground reflection was measured below 10 m. The start altitude is set to 700 m (shortly before Outer Marker altitude) and the descending rate is chosen to be 3.5 m/s, which is close to the one of a standard ILS approach. The signal-to-noise-ratio C/N_0 is assumed to be 45 dB-Hz if not stated otherwise. As reference please notice the following characteristics of an ILS approach (according to [6], meter and kilometer values only approximate):

Standard ILS Approach: Glide path: 2-3°, Sink rate around 3.5 m/s		
Marker	Distance from runway	Altitude
Outer Marker OM	4-7 mi / 6,5-11 km	730-1900 ft / 220-580m
Middle Marker MM	3250-3750 ft / 1000-1150m	200 ft / 60 m
Inner Marker IM	1000 ft / 300 m	100 ft / 30 m

Table 1: ILS characteristic glide slope values

The simulator’s signal generator uses the following common signal settings:

GPS L1 C/A	Galileo E5 AltBOC(15,10)
<ul style="list-style-type: none"> • Gold Code of length 1023 • Bandwidth: 10 MHz (one-sided) • Code chip rate 1.023 MChips/s • Integration time: 1 ms 	<ul style="list-style-type: none"> • Primary code of length 10 230 • Bandwidth: 45 MHz (one-sided) • Code chip rate 10.230 MChips/s • Integration time: 1 ms

Table 2: Signal characteristics

For the Galileo scenario, the receiver was set to track the E5b data component, i.e., the E5b,I signal, which is expected to be used by aviation and other SoL applications.

The DLL and PLL parameters are set to the following usual values:

DLL parameters:	PLL parameters:
<ul style="list-style-type: none"> • Early-Late Correlator spacing: 1 code chip (standard) or 0.1 code chip (narrow correlator) • DLL type: Non-coherent, 2nd order • Bandwidth B_{Loop}: 2 Hz • Damping Factor ξ: 0.707 	<ul style="list-style-type: none"> • Costas PLL, 2nd order • Bandwidth B_{PLL}: 10 Hz • Damping Factor ξ: 0.707

Table 3: Tracking loop parameters

4. SIMULATION RESULTS

This section presents the results of computer simulations of the code tracking performance for the scenarios defined above. For comparison, the simulated receiver performance in absence of multipath is given. Then the error behaviour during a typical landing approach is shown. Simulation results for different elevation and azimuth angles are then

presented in order to identify critical values of these angles. The simulations deliver the σ (standard deviation) and the bias (mean) of the pseudo-range (delay) error. For clarity, the pseudo-range values are presented in terms of meters instead of seconds, assuming a constant propagation speed c_0 , the speed of light.

For the most critical values of elevation and azimuth, more intensive simulations have been carried out. In addition to standard deviation and mean values an analysis of the complete error distribution is carried out. On base of the latter it is possible to draw conclusions on the occurrence rate of most critical error events that happen rarely but have a much larger magnitude than indicated by the average performance measurement.

4.1 PERFORMANCE WITHOUT MULTIPATH

Table 4 shows the receiver performance that has been simulated in absence of multipath (AWGN channel model, averaged over 30 minutes simulation time). It has to be noted, that because of limited resources only two navigation signals could be evaluated. GPS L1 C/A has been chosen because of its already long time existence and Galileo E5b,I because of the higher bandwidth compared to Galileo L1 signal and the different carrier frequency.

	GPS L1 C/A	GPS L1 C/A narrow	Galileo E5b,I
C/N_0 [dB-Hz]	Standard deviation of pseudo-range error [m]		
35	6.69	1.55	1.99
40	3.24	0.780	0.800
45	1.73	0.414	0.371
50	0.953	0.227	0.195
55	0.530	0.133	0.107
60	0.291	0.0738	0.0583
65	0.166	0.0414	0.0326
70	0.0949	0.0231	0.0186

Table 4: Receiver performance for AWGN channel (no multipath)

4.2 TYPICAL TRACKING ERROR BEHAVIOUR DURING APPROACH

The delay tracking error over time during an example approach is shown in Figure 4. The simulations without noise allow to see the effect of multipath on the performance. It can be observed, that the largest errors occur when there is a strong ground echo (the corresponding amplitudes are plotted in Figure 5). Interestingly, positive errors tend to occur more frequently than negative ones, especially if their magnitude is high. An explanation of this effect will be given in Section 5.

At a C/N_0 of 45 dB/Hz much of the multipath error is hidden within the noise, but still errors of large magnitude occur occasionally. The contribution of the largest errors to the average performance may be relatively small, especially if they are processed by further averaging techniques like carrier smoothing. On the other hand, in view of integrity requirements, one can also conclude that average performance quantities, like mean or standard deviation, do not sufficiently characterize the most critical error events. Other measures, like the maximum error or the complete error distribution, become of interest in such a context.

In a multipath mitigation study carried out within the ANASTASIA project, efficient maximum likelihood estimation methods have been investigated [7][8]. Simulations with the ASCM show that the ground echo influence can be mitigated successfully.

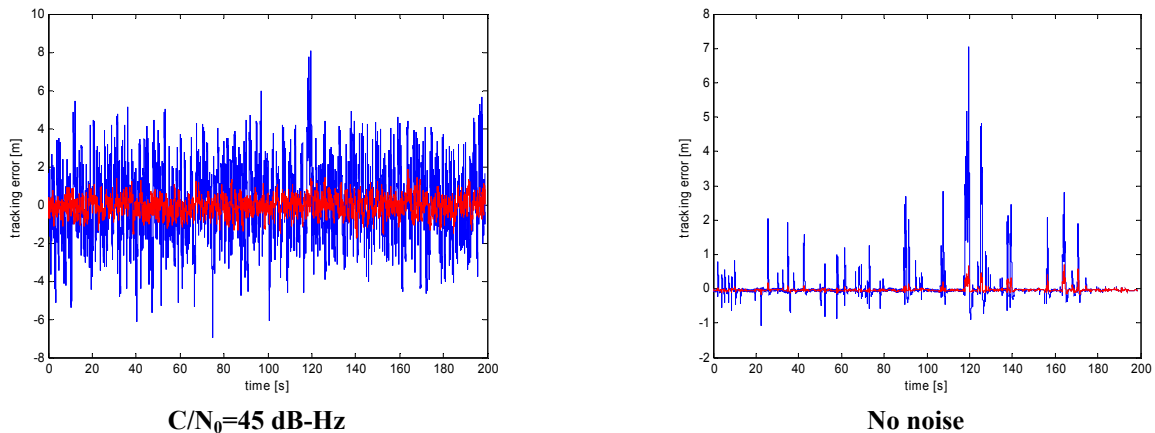


Figure 4: Tracking error for GPS L1 C/A signal (A340). Standard (blue) and narrow correlator (red)

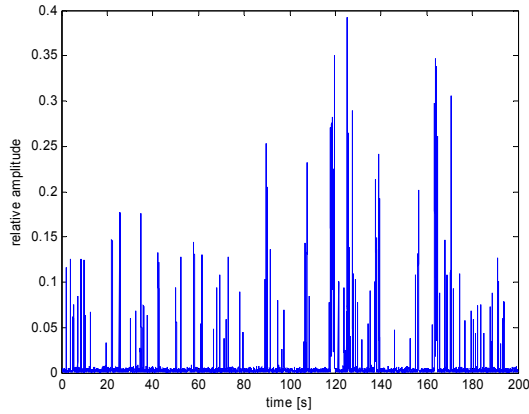


Figure 5: Strength of the ground echo during an example approach

4.3 INFLUENCE OF AIRCRAFT TYPE

This section presents the tracking performance as function of azimuth γ and elevation θ (see Figure 6), using the ASCM. Since the critical azimuth and elevation values are not expected to depend on the navigation signal type, the simulations were carried out for the GPS L1 C/A code only. The two aircraft are compared while the type of plane is affecting the shape of the Doppler power spectrum for diffraction effects and fuselage reflections [3] in the ASCM.

The results are plotted in polar azimuth-elevation plots, whose interpretation is corresponding to Figure 6. Due to the ASCM limitations the results cover an elevation range from 10° to 70° and an azimuth range from 10° to 170° and 190° to 350° . The limitations of the angular values arise from the physical optics model that underlies the ASCM, where the fuselage is modelled as a cylinder [3]. Due to that fact physical reasonable ASCM outputs are obtainable only for restricted angular ranges.

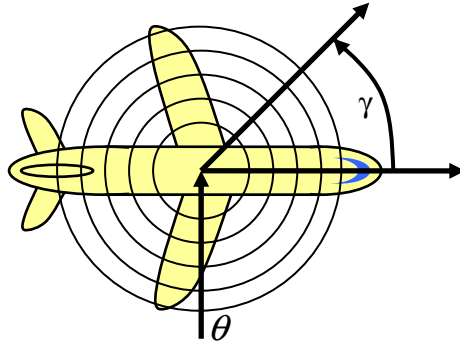


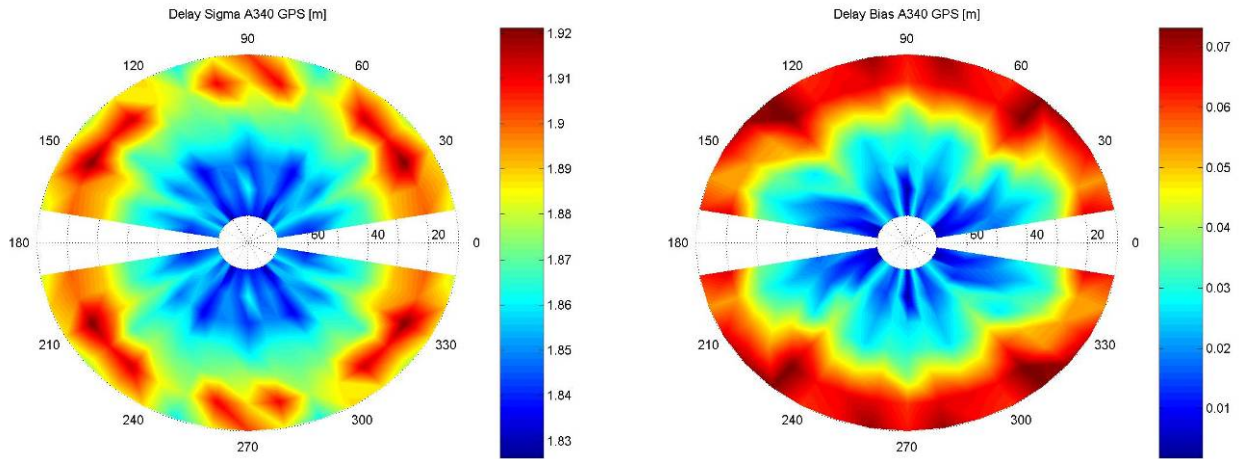
Figure 6: Azimuth-elevation plot, azimuth angle γ and elevation angle θ

Figure 7 and Figure 8 show the standard deviation and bias of the simulated pseudo-range error for the A340 and the VFW614 aircraft, respectively. All simulation results are averaged over 30 approach simulation runs, whereas a resolution of 5 degree steps for azimuth and a resolution of 10 degree steps for elevation are used. In these plots, to improve the statistics, the two symmetry axes are taken into account, resulting in 120 approaches per data point effectively.

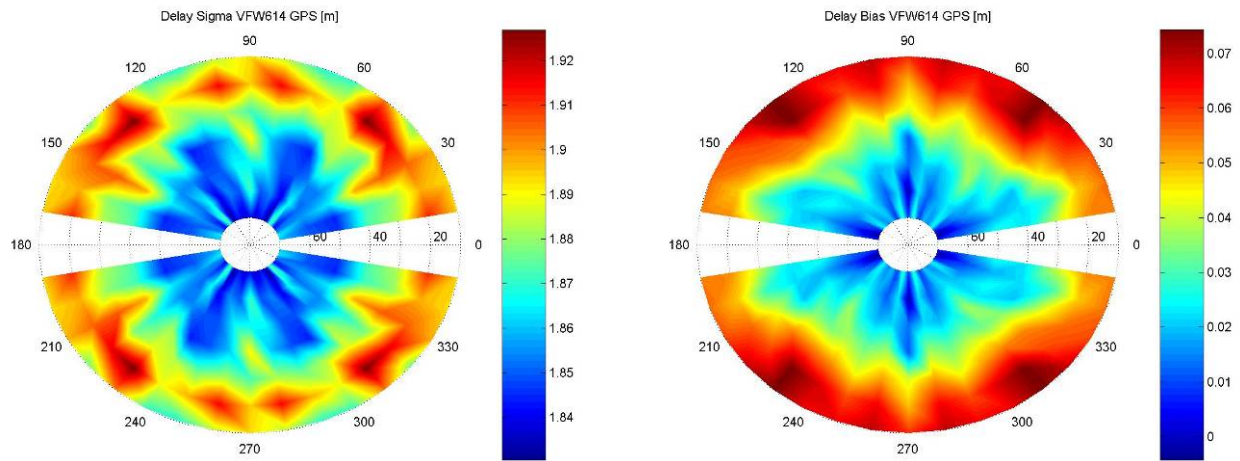
A comparison of Figure 7 and Figure 8 in terms of aircraft type shows no significant difference on the pseudo-range error, especially if the effect of statistical variations due to limited simulation time is taken into account. As expected, the delay error bias and variance generally decreases with an increasing elevation angle. The dependence on azimuth is less pronounced, but the most critical regions appear to be around $\pm 45^\circ$ and $\pm 135^\circ$. It can also be seen that the error bias is much smaller than the standard deviation. The most critical scenarios in terms of azimuth and elevation are summarized in Table 5. These values are critical for a standard ILS approach (as described in Section 3) whereby effects, like fuselage reflection and ground echo are considered.

	A340	VFW614
Most Critical Azimuth Angles	$\approx 45^\circ, \approx 135^\circ, \approx 225^\circ, \approx 315^\circ$	
Most Critical Elevation Angles	10°	

Table 5: Critical scenarios in terms of azimuth angle γ and elevation angle θ



Standard deviation of the pseudorange error [m] **Bias of the pseudorange estimate [m]**
Figure 7: Standard deviation and bias over azimuth and elevation, A340



Standard deviation of the pseudorange error [m] **Bias of the pseudorange estimate [m]**
Figure 8: Standard deviation and bias over azimuth and elevation, VFW614

4.4 DISTRIBUTION OF PSEUDO-RANGE ERROR

From the simulations of 200 approaches per data point at azimuth $\gamma=135^\circ$ and elevation $\theta=10^\circ$, already considered in the previous section, we now investigate the distribution $p(\epsilon)$ of the pseudo-range error ϵ . For different carrier-to-noise ratios C/N_0 histograms of the measured pseudo-range errors have been computed to determine the error occurrence rates over the simulated approaches. The distributions refer to the measurements during all the 200 approaches.

4.4.1 GPS L1 C/A SIGNAL

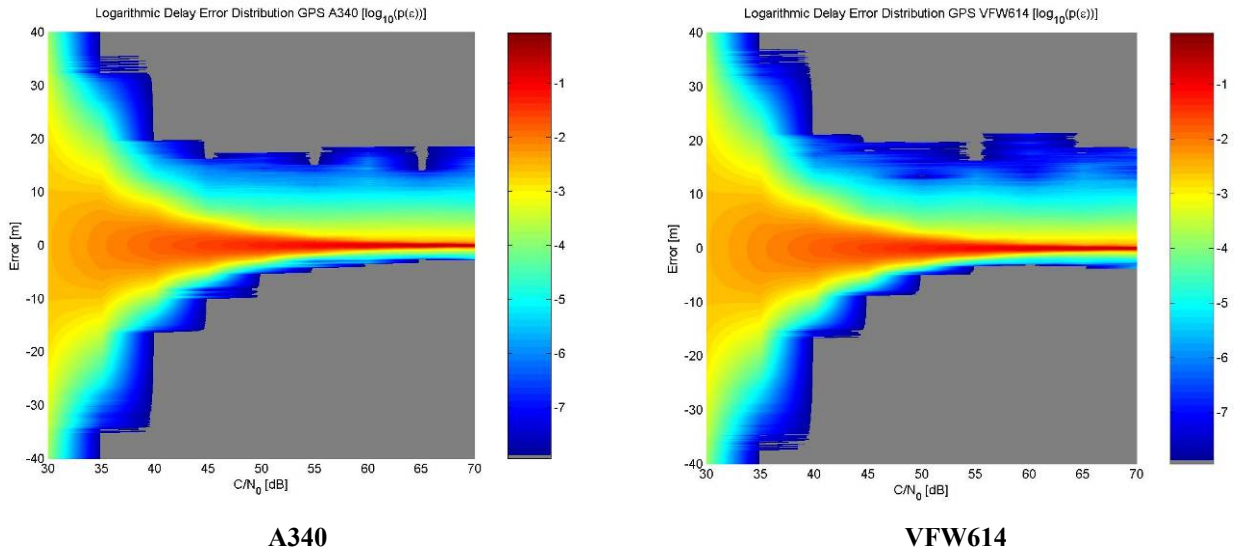


Figure 9: GPS L1 C/A : Distribution of pseudorange error during simulated flights

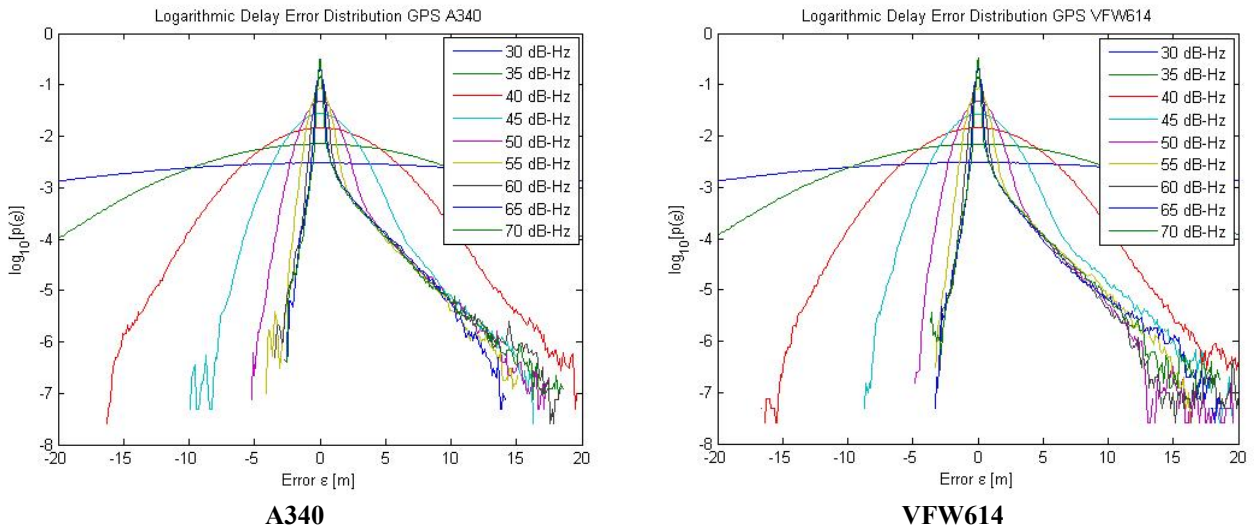


Figure 10: GPS L1 C/A: Pseudorange error distribution for different C/N_0

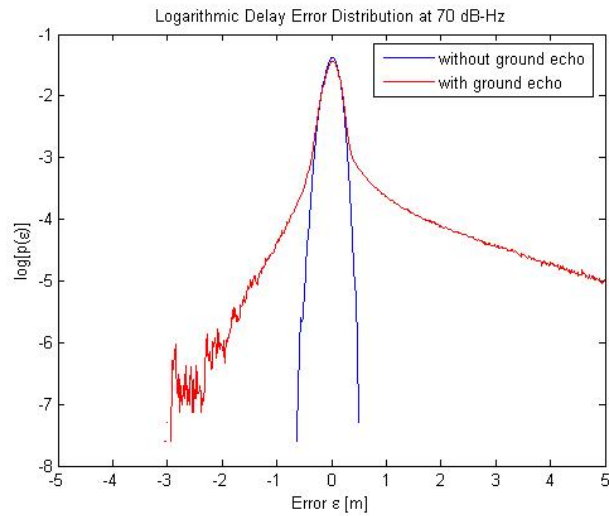


Figure 11: Influence of ground echo: A340, pseudo-range error distribution at 70 dB-Hz.

Figure 9 shows the logarithmic delay error distribution over C/N_0 . It illustrates the same flattening effect as observed in the previous section. It is also possible to see that positive delay errors occur more frequently than negative ones, as observed for the example approach in Figure 4.

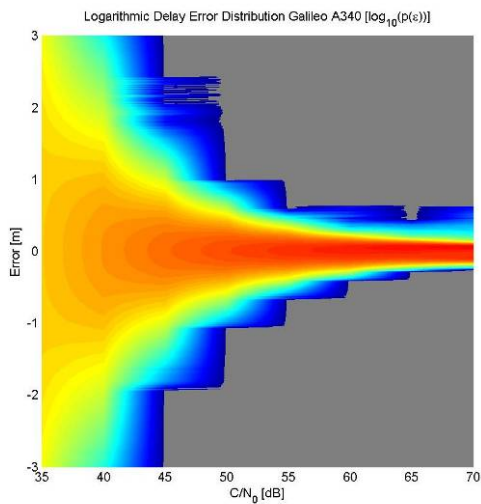
Using the same data, Figure 10 shows the distributions as individual curves for different C/N_0 values. These curves show clearly that the delay error does not follow a Gaussian distribution, especially if the error magnitude is high. Simulations where the ground echo of the ASCM is switched off show (see Figure 11) that the particular shape of the error distributions is mostly caused by the ground multipath. A theoretical analysis of these error events, given in Section 5, confirms the observed behaviour. From the tails of the error distributions it is possible to calculate the magnitude of critical error events with a particular occurrence rate, as given in Table 6.

Error magnitude at		10^{-2} occurrence rate	10^{-6} occurrence rate
45 dB-Hz	A340	> 4.6 m	> 15.5 m
	VFW614	> 4.7 m	> 17.7 m
70 dB-Hz	A340	> 1.9 m	> 17.7 m
	VFW614	> 2.0 m	> 17.9 m
	A340, no ground echo	> 0.30 m	> 0.58 m

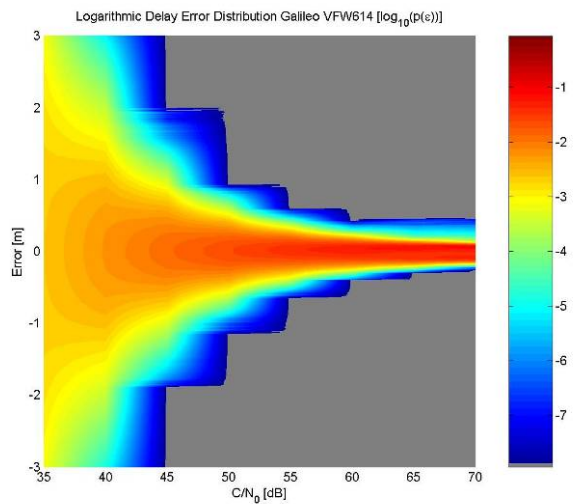
Table 6: GPS L1 C/A: Magnitude of critical error events

4.4.2 GALILEO E5B SIGNAL

A comparison of Figure 12 and Figure 13 with Figure 9 and Figure 10 shows that due to the improved signal structure the Galileo E5b signal is more robust against multipath, which can be easily seen by comparing the width of the shown distribution $p(\epsilon)$.

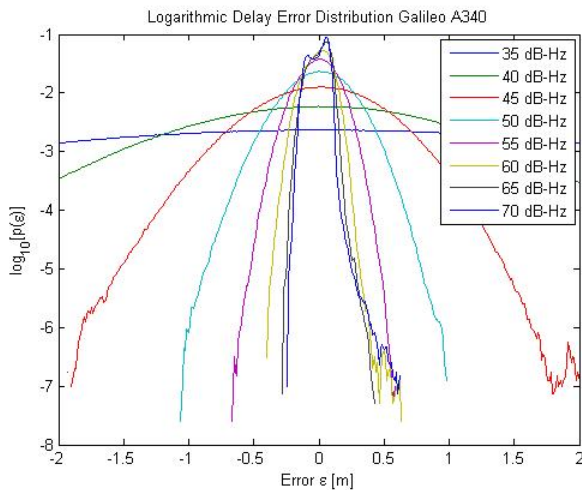


A340

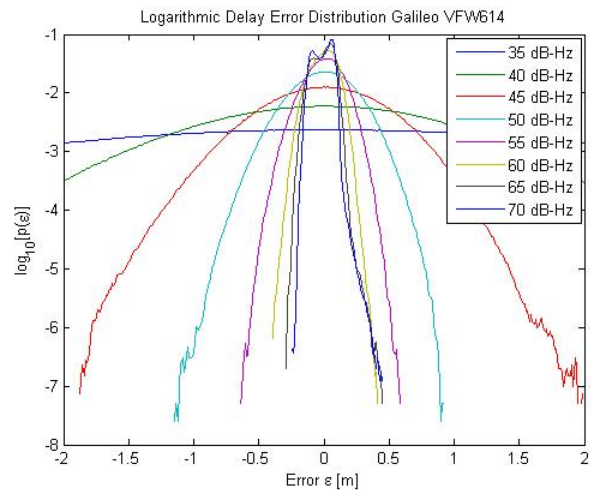


VFW614

Figure 12: Galileo E5b : Distribution of pseudorange error during simulated flights



A340



VFW614

Figure 13: Galileo E5b: Pseudorange error distribution for different C/N_0

Error magnitude at		10^{-2} occurrence rate	10^{-6} occurrence rate
45 dB-Hz	A340	> 0.99 m	> 2.2 m
	VFW614	> 0.99 m	> 1.9 m
70 dB-Hz	A340	> 0.14 m	> 0.55 m
	VFW614	> 0.14 m	> 0.39 m

Table 7: Galileo E5b: Magnitude of critical error events

4.4.3 GPS L1 C/A: NARROW CORRELATOR

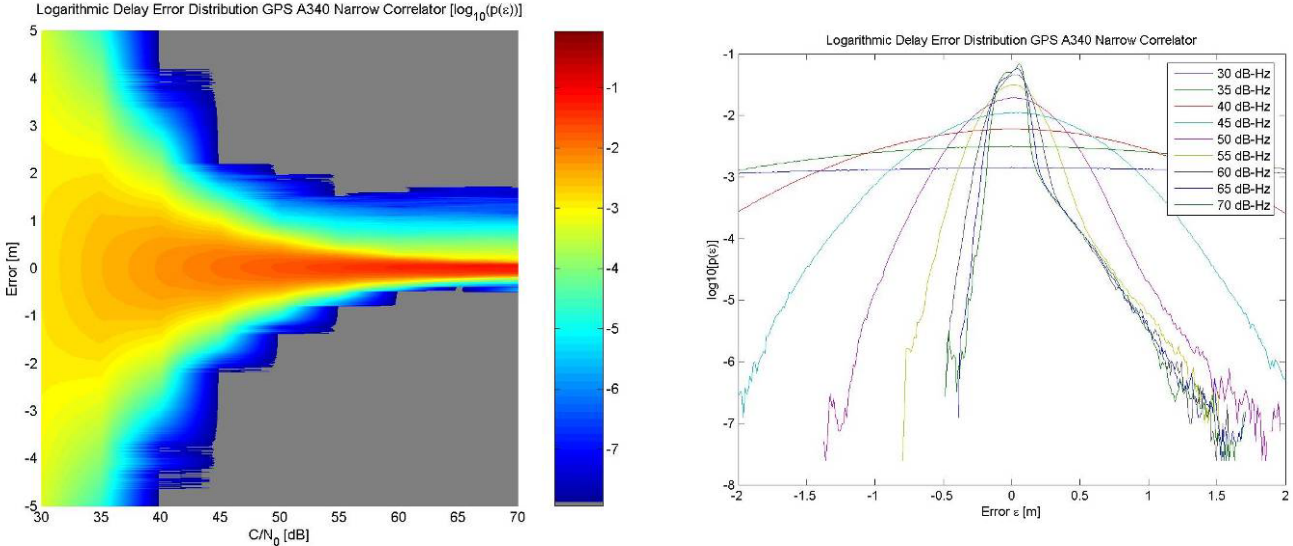


Figure 15: Narrow correlator: pseudorange error distribution for different C/N_0

Error magnitude at	10^{-2} occurrence rate	10^{-6} occurrence rate
45 dB-Hz, A340	> 1.1 m	> 2.1 m
70 dB-Hz, A340	> 0.22 m	> 1.5 m

Table 8: Narrow correlator: Magnitude of critical error events

5. THEORETICAL ANALYSIS OF PSEUDO-RANGE ERROR DISTRIBUTION

In this section a theoretical approximation of the pseudo-range error distribution is derived and presented for the GPS L1 C/A signal. As the ground echo appears to dominate the multipath error (see Figure 11), the diffractive component of the direct path and the fuselage echo are neglected. Furthermore, the considered model is based on some assumptions that simplify the calculations, as an exact analysis of the dynamic error behaviour of the tracking loop in presence of multipath is difficult. Although these calculations can only give an approximation of the true error, the analysis serves as a valuable tool to explain and confirm the observations made from the simulation results.

For the static case, the noiseless multipath error (bias) caused by a single reflection can easily be determined from the multipath error envelope. Figure 16(a) shows this error as a function of the relative (direct-to-multipath) delay for different relative phases and magnitude of the relative amplitude $a=0.5$. Also shown is the result of averaging uniformly over all phase values. It is interesting to see that this average error has different symmetry as the error envelope. In particular, the positive errors are more pronounced than the negative ones, like it has been observed in the simulation results. Since the phase of the ground echoes is changing quickly, a similar averaging effect is caused within the DLL. The phase averaged multipath error bias as function of delay and amplitude is given in Figure 16(b).

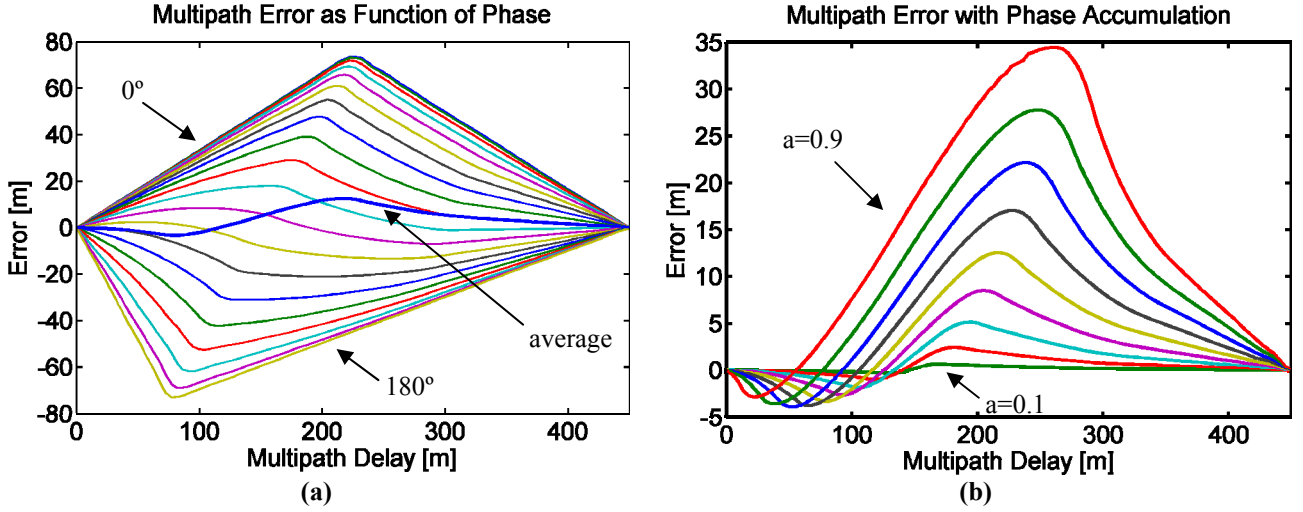


Figure 16: Multipath error bias for (a) different phases and relative amplitude $a=0.5$ (b) for averaged phase

In the ASCM the generation of the ground echo is driven by a Markov chain, where the transition matrix depends on the altitude level (see Section 2). For a given altitude level l , the probability density function (PDF) of the magnitude of the amplitude a can be written as

$$p(a | l) = \sum_{v=1}^4 p(a | v, l) \cdot P(v | l) \quad (2)$$

where v denotes the state of the Markov chain. For a sufficiently long flight, the probability $P(v | l)$ for the state of the level l Markov chain follows from its steady state vector, which can be calculated from the corresponding transition matrix. For a given state v the magnitude of the amplitude can be modelled by the Rayleigh distribution, i.e.,

$$p(a | v, l) = p(a | v) = \frac{a}{\bar{P}_v} \exp\left(-\frac{a^2}{2\bar{P}_v}\right) \quad (3)$$

Where \bar{P}_v is the power associated with state v . Note that the altitude levels differ in the Markov transition probabilities only and not in the power levels. The particular Doppler power spectrum of the delay, which is part of the ASCM, is not taken into account in this model.

The joint PDF of amplitude and delay d is given by

$$p(a, d) = \sum_{l=1}^3 p(a | l) \cdot p(d | l) \cdot P(l) \quad (4)$$

where the probability $P(l)$ follows from the fraction of time the airplane is within level l to the simulated time. Assuming a constant sink rate, $p(d | l)$ represents a uniform distribution over the delays corresponding to the altitude interval, where the delay d is related with altitude h and elevation angle θ by

$$d = 2h \sin(\theta) \quad (5)$$

Let $\varepsilon_{MP}(a, d)$ denote the phase averaged multipath error shown in Figure 16(b), which represents the pseudo-range error of a DLL in lock state in the absence of noise. The influence of noise is now modelled additively by

$$\varepsilon = \varepsilon_{MP}(a, d) + n, \quad n \sim N(0, \sigma^2) \quad (6)$$

which presumes that the error component caused by the noise is Gaussian distributed and independent of the multipath. The variance of the error is determined by simulations for the AWGN channel (compare Table 4). The distribution of the tracking error is then equal to

$$p(\varepsilon) = \iint_{a, d} p(\varepsilon | a, d) \cdot p(a, d) \, dd \, da \quad (7)$$

where

$$p(\varepsilon | a, d) = \frac{1}{\sqrt{2\pi\sigma^2}} \exp\left(-\frac{(\varepsilon - \varepsilon_{MP}(a, d))^2}{2\sigma^2}\right) \quad (8)$$

For the GPS L1 C/A signals the approximate tracking error, calculated according to (7), is compared in Figure 17 and Figure 18 with the respective simulation results. Despite of all the simplifying assumptions within the underlying model, the calculations match remarkably well with the simulations. And even though the rough additive model in (6) is used, the calculations confirm the observation that the tail of the error distribution is not Gaussian. This result is very interesting in the integrity context. For high SNR one can see that the approximated distribution results in smaller errors than those from the simulations. This shows that the conditions the model is based on are still relatively optimistic compared to the true dynamic tracking process. An advantage of the theoretical approximation is that it allows to estimate the occurrence rate of critical error events beyond the order that is feasible for analysis by computer simulation. Corresponding values are shown in Table 9.

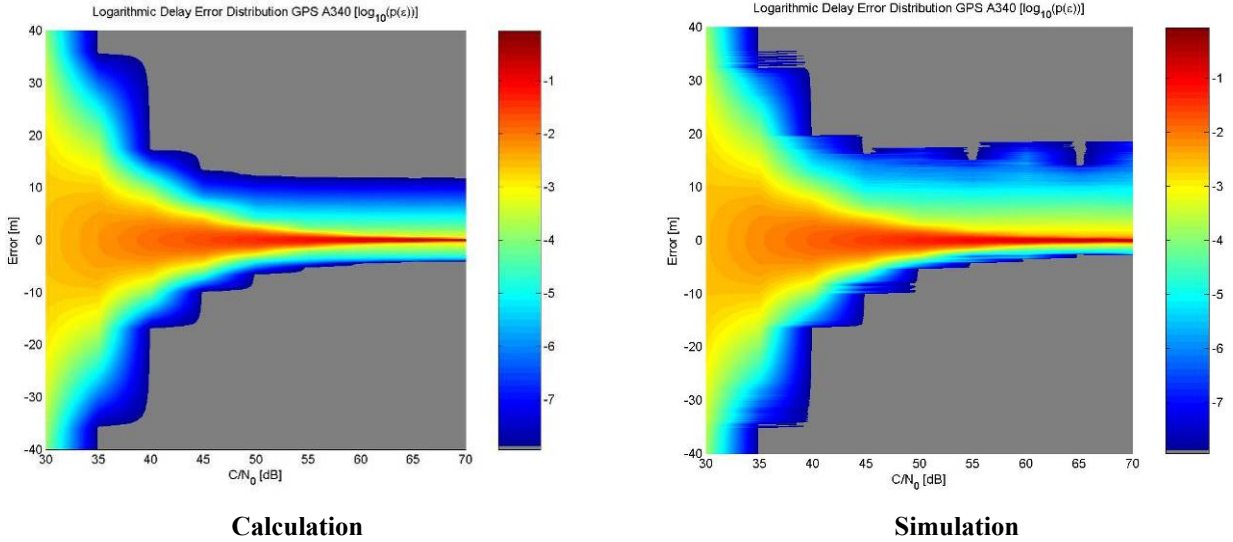


Figure 17: Comparison of pseudorange error distributions

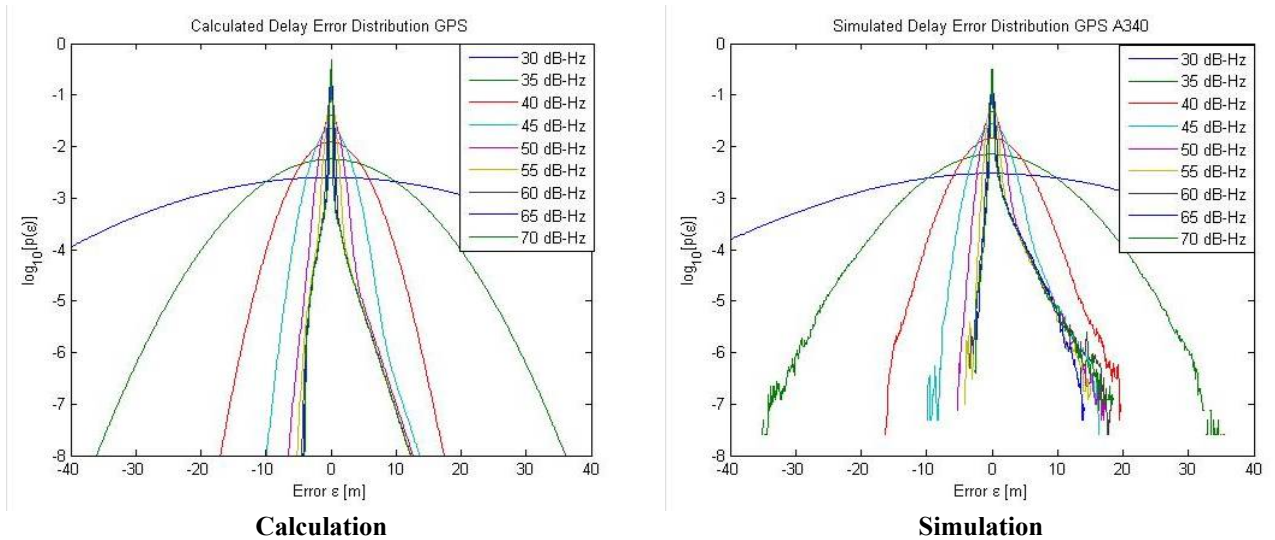


Figure 18: Comparison of pseudorange error distributions for different C/N₀

Error magnitude at	10 ⁻² occurrence rate	10 ⁻⁶ occurrence rate	10 ⁻⁹ occurrence rate	10 ⁻¹² occurrence rate
45 dB-Hz	> 4.60 m (Simulation: >4.6 m)	> 11.20 m (Simulation: >15.5 m)	> 18.40 m	> 24.90 m
70 dB-Hz	> 0.600 m (Simulation: >1.9 m)	> 9.70 m (Simulation: >17.7 m)	> 16.70 m	> 23.10 m

Table 9: Calculated magnitudes of critical error events

6. CONCLUSIONS

The results of the assessment reveal that the size of the plane as well as the azimuth of the satellite constellation is not important while the elevation of the satellite plays the major role for the pseudo-range error distribution. The most critical pseudo-range errors are caused by the ground echo path. Due to the variations of these echoes during an approach their contribution is not permanent. Instead, errors of extraordinarily high magnitude occur from time to time. Further investigations show that the pseudo-range error distribution is non-symmetric around the true pseudo-range. It is characterized by a long tail towards positive values. In the development of aircraft landing systems it is quite common to over bound the true error distribution by a wider Gaussian distribution. Nevertheless, it cannot be proven that this overbounding is sufficient for very low occurrence rates. Furthermore our results show, that these over bounding distributions have significantly larger standard deviations than the true standard deviation of the process. The knowledge of such over bounding distributions is very important for the certification of the final landing system.

ACKNOWLEDGMENTS

This work was conducted within the ANASTASIA project. ANASTASIA (Airborne New and Advanced Satellite techniques and Technologies in A System Integrated Approach) is an integrated project which receives funding from the European Community's Sixth Framework Program (DG research); see www.anastasia-fp6.org.

REFERENCES

- [1] A. Steingass, A. Dreher, L. Greda, E. Schittler-Neves, A. Konovaltsev, C. Weber, A. Lehner, M. Lentmaier, B. Krach, E. Kubista, T. Prechtel, M. Schönhuber, N. Witternigg, F. Pérez-Fontán, S. Serrano García, B. Sanmartín Pérez, A. Escolar Piedras, A. Thain, C. Baroux, E. Walter, *Characterization of Critical Environment*, ANASTASIA D5.1, 2006.
- [2] A. Steingass, A. Lehner, "Aeronautical Channel Model", available at <http://www.kn-s.dlr.de/satnav>.
- [3] A. Steingass, A. Lehner, F. Pérez-Fontán, E. Kubista, M.J. Martín, B. Arbesser-Rastburg, "The High Resolution Aeronautical Multipath Navigation Channel", *ION NTM 2004*, January 26-28, in San Diego, California USA.
- [4] ITU Recommendation ITU-R 682-1, "Propagation Data Required for the Design of Earth-Space Aeronautical Mobile Telecommunication Systems", International Telecommunication Union, February 2007.
- [5] Macabiau, C., Moriella, L., Raimondi, M., Dupouy, C., Steingass, A., Lehner, A., "GNSS Airborne Multipath Errors Distribution Using the High Resolution Aeronautical Channel Model and Comparison to SARPs Error Curve", *Institute of Navigation National Technical Meeting ION NTM 2006*, Monterey, USA, January 18-20, 2006.
- [6] M. Kayton, W. R. Fried. *Avionics Navigation Systems*, 2nd edition, John Wiley & Sons, Inc., New York 1997.
- [7] A. Konovaltsev, O. Esbri Rodriguez, M. Lentmaier, C. Macabiau, M. Raimondi, C. Martel, D. Moore, M. Philippakis, P.-Y. Dumas, S. Monroq, *Interference and Multipath Mitigation Study Report*, ANASTASIA D3.2.1.1, 2006.
- [8] B. Krach, M. Lentmaier, "Efficient Soft-Output GNSS Signal Parameter Estimation using Signal Compression Techniques", *3rd ESA Workshop on Satellite Navigation User Equipment Technologies - NAVITEC '2006*, Noordwijk, Netherlands, 2006-12-11 - 2006-12-13.